Tribol Lett (2015) 60:21
DOI 10.1007/s11249-015-0599-x

ORIGINAL PAPER

# Influence of Potential Shape on Constant-Force Atomic-Scale Sliding Friction Models

**Octavio J. Furlong[1] · Sergio J. Manzi[1] · Ashlie Martini[2] · Wilfred T. Tysoe[3]**

Received: 17 July 2015 / Accepted: 21 September 2015 / Published online: 14 October 2015


**Abstract** The majority of atomic-scale friction models in which sliding is proposed to occur over the atomic-scale energy corrugation at the sliding interface assume a simple sinusoidal potential. An analysis of these models shows that the energy barrier is reduced by the imposition of an external force $F$, becoming zero at a critical force defined as $F^*$. It was first suggested by Prandtl that the energy barrier approaches a limiting value with a force dependence that is proportional to $(F^* - F)^{3/2}$. In order to explore the effects of the shape of the energy potential on the sliding behavior, this model is analyzed for constant-force sliding with a non-sinusoidal potential of the form $\sin^n\left(\frac{\pi x}{a}\right)$, where $n$ is an even integer $\geq 2$. The same asymptotic dependence is found as suggested by Prandtl, where the proportionality constant depends on the shape of the potential. These results are used to calculate the velocity and temperature dependences of sliding friction for constant-force sliding over non-sinusoidal surface potentials.

**Keywords** Sliding friction · Prandtl–Tomlinson model · Velocity dependence · Temperature dependence

✉ Wilfred T. Tysoe
wtt@uwm.edu

[1] INFAP/CONICET, Universidad Nacional de San Luis, Ejército de los Andes 950, 5700 San Luis, Argentina

[2] School of Engineering, University of California Merced, Merced, CA 95343, USA

[3] Department of Chemistry and Biochemistry and Laboratory for Surface Studies, University of Wisconsin-Milwaukee, 3210 N Cramer Street, Milwaukee, WI 53211, USA

## 1 Introduction

The first analysis of the influence of an external force on the energy barrier of a thermally activated process was performed in 1928 by Prandtl [1] to examine the inelastic stress–strain behavior of materials. Prandtl also indicated that the model could be applied equally well to friction. Tomlinson later pointed out that a surface sliding potential could arise from the atomic-scale potential corrugation [2], and this friction model is now known as the Prandtl–Tomlinson (PT) model. The PT model analyzes the effect of an external compliant force, which is coupled through a spring to a simple periodic sinusoidal potential on the energy barrier height between adjacent minima. With the introduction of the atomic force microscope (AFM) for friction measurements [3, 4], it was realized that the PT model could be directly applied to AFM experiments, and it has been widely used to model velocity and temperature dependences of nanoscale sliding friction [5–11].

Similar concepts were used in 1936 by Eyring to model viscosity [12, 13] using transition state theory [14] with constant-force sliding by considering liquid flow as a unimolecular reaction in which the elementary process consists of a molecule in the fluid passing from one equilibrium position to another over an energy barrier under the influence of a constant shear force, where again the sliding potential is considered as a simple periodic function. Eyring assumed that the rate constant $k(F)$ is given by $k(F) = k_0 e^{\frac{Fd}{k_B T}}$, where $k_0$ is the rate constant for the process in the absence of an external force, $F$ is the lateral force, $k_B$ is the Boltzmann constant and $T$ the absolute temperature. This model essentially assumes that the shape of the energy profile is not modified by the imposition of an external force. Here, an external force $F$ exerted on the

system to displace it a distance $x$ reduces the activation barrier by $Fx$. When $x = d$, the distance from the initial minimum to the first maximum (the transition state), the energy barrier decreases to zero to yield a force-dependent energy barrier given by $\Delta E(F) = E_0 - Fd$ to give the above rate equation. This approach has the advantage that the analysis is independent of the energy barrier shape.

Similar models have been applied to describe mechanochemical reaction rates in the so-called Bell model [15]. Efforts have been made to take account of the influence of the potential shape in the extended Bell model [16]. This analysis separately expands the potential energy curve as Taylor series about the initial and transitions state, resulting in a quadratic force correction to the model: $\frac{\chi_{TS}-\chi_{IS}}{2}F^2$, where $\chi_{TS}$ and $\chi_{IS}$ are the mechanical compliances (the inverse of the force constants) at the transition and initial states, respectively. Since the initial and transitions states are modeled separately, the theory does not capture the behavior as the activation barrier becomes small. However, because of its simplicity, approaches similar to that taken in the Bell model have been used to study a wide range of tribological behavior for constant force rather than compliant sliding, including rubber [17, 18] and mica friction [19], friction modifiers [20], the friction of monolayers of fatty acid soaps in glass/mica contacts [21], fracture [22], and to describe dissolution [23] and nanoscale wear rates measured in an AFM [24–28]. The similarity between these models has recently been discussed in detail [29].

While Prandtl's work explores the linear response at low force, he also derives asymptotic solutions at large forces by analyzing the force–distance curve as the end of the compliant spring moves a distance $x_0$ to reduce the height of the energy barrier to zero. By considering the shape of the force–distance curve as $x$ approaches $x_0$, it is shown that the energy barrier $\Delta E(x)$ varies as a function of spring position $x$ as $\Delta E(x) \propto (x - x_0)^{3/2}$. Designating the force at $x = x_0$ to be $F^*$ and assuming that the force is dominated by the motion of the end of the spring gives $\Delta E(F) = \frac{1}{\beta}(F^* - F)^{3/2}$, where the proportionality constant $\beta$ depends on the shape and height of the energy barrier; this approach has been used to model sliding in AFM [5, 8, 30].

The influence of the shape of the energy barrier on frictional behavior of the PT model has been analyzed using kinetic Monte Carlo simulations [10, 31] and the master equation method [32]. However, since, as indicated above, constant-force sliding models are more prevalent than those for compliant sliding, in this paper, we explore the asymptotic behavior as $F$ approaches $F^*$ for constant-force sliding as a function of the shape of the potential using a model potential of the form $\sin^n\left(\frac{\pi x}{a}\right)$. This type of surface potential has been previously used to fit AFM friction results on mica, providing much more accurate fits to experiment than the classical sinusoidal potential [30]. Here, we derive analytical expressions for the lateral force due to these non-sinusoidal potentials, which complement the previous work done using Monte Carlo simulations. The derivation is carried through to the point where the presented equations can be used to characterize the velocity and temperature dependences of friction. A similar analysis has already been carried out for a simple sinusoidal potential under rigid sliding conditions [29].

## 2 Results and Discussion

### 2.1 Sliding Energy Barrier

We analyze the variation in barrier height as a function of force by assuming constant-force sliding with a force $F$. In this case, the potential due to the external force is given by $V(x) = -Fx$, where $x$ is a distance along the surface. We consider sliding over a periodic, non-sinusoidal potential $\sin^n(\pi x/a)$ which yields peaked structures for even integer values of $n \geq 2$. Figure 1 illustrates how the sharpness of the potential is determined by the value of the parameter $n$.

Prandtl demonstrated that, in general, the energy barrier varies as $\Delta E(F) = \frac{1}{\beta}(F^* - F)^{3/2}$ where $F^*$ is a critical force at which the barrier is reduced to zero. The goal here is to show that similar behavior occurs for constant-force sliding and to calculate the proportionality constant $\beta$ for

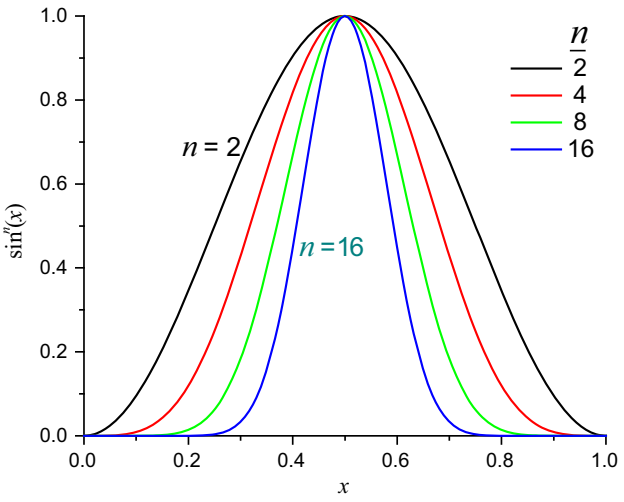


**Fig. 1** The shape of the non-sinusoidal periodic potential is determined by the exponent $n$

sliding potentials with different shapes. We write the combined potential at some constant force $F$ as:

$$V(x,F) = E_0 \sin^n\left(\frac{\pi x}{a}\right) - Fx \tag{1}$$

where $E_0$ is the amplitude of the sliding potential, and $a$ the periodicity.

The imposition of the external force lowers the energy barrier between adjacent stable positions, and the turning points at some external force $F$ are calculated by differentiating Eq. (1), so that:

$$\frac{\mathrm{d}V(x,F)}{\mathrm{d}x} = \frac{n\pi E_0}{a}\sin^{(n-1)}\left(\frac{\pi x}{a}\right)\cos\left(\frac{\pi x}{a}\right) - F = 0 \tag{2a}$$

The force required to lower the barrier height ($\Delta E$) to zero defines the critical force $F^*$ which occurs at a position $x^*$:

$$\frac{n\pi E_0}{a}\sin^{(n-1)}\left(\frac{\pi x^*}{a}\right)\cos\left(\frac{\pi x^*}{a}\right) = F^* \tag{2b}$$

Furthermore, the inflection point at the critical position $x^*$ satisfies:

$$\left.\frac{\partial^2 V}{\partial x^2}\right|_{F^*} = \frac{n\pi^2 E_0}{a^2}$$
$$\left[(n-1)\sin^{(n-2)}\left(\frac{\pi x^*}{a}\right)\cos^2\left(\frac{\pi x^*}{a}\right) - \sin^n\left(\frac{\pi x^*}{a}\right)\right] = 0 \tag{3a}$$

yielding an equation for $x^*$ as:

$$(n-1)\sin^{(n-2)}\left(\frac{\pi x^*}{a}\right)\cos^2\left(\frac{\pi x^*}{a}\right) = \sin^n\left(\frac{\pi x^*}{a}\right) \tag{3b}$$

This can be solved to give $\sin\left(\frac{\pi x^*}{a}\right) = \sqrt{\frac{n-1}{n}}$, and $\cos\left(\frac{\pi x^*}{a}\right) = \sqrt{\frac{1}{n}}$; and therefore $x^* = \frac{a}{\pi} a \cos\left(\frac{1}{n^{\frac{1}{2}}}\right)$.

Substituting into Eq. (2b) gives:

$$F^* = \frac{n\pi E_0}{a}\left(\frac{n-1}{n}\right)^{n/2}\left(\frac{1}{n-1}\right)^{1/2} \tag{4}$$

In order to study the asymptotic behavior of $\Delta E$ as it approaches zero, we perform a Taylor series expansion of Eq. (1) around ($x^*$, $F^*$), obtaining:

$$V(x-x^*, F-F^*) = E_0\left(\frac{n-1}{n}\right)^{n/2}$$
$$\left[1 - \frac{\pi^3}{3a^3}\frac{n^2}{(n-1)^{1/2}}(x-x^*)^3 + \cdots\right] + x(F^*-F) - x^*F^* \tag{5}$$

Figure 2 compares Eq. (1) (black dashed line) with Eq. (5) (blue solid line) as a function of $F$ for a system with typical values of $n = 8$, $a = 1 \times 10^{-9}$ m, $E_o = 1 \times 10^{-20}$ J, and therefore $F^* = 5.5683 \times 10^{-11}$ N and the expansion in Eq. (5) is reasonable for small deviations from $F^*$.

The height of the energy barrier $\Delta E$ is calculated as a function of $F$ from the turning points of Eq. (5) from which the position of the maximum and minimum that define $\Delta E$ can be calculated as follows:

$$x_{\min} = -\sqrt{\frac{a^3}{E_0\pi^3}\left(\frac{n}{n-1}\right)^{n/2}\frac{(n-1)^{1/2}}{n^2}(F^*-F)} + x^* \tag{6a}$$

and

$$x_{\max} = \sqrt{\frac{a^3}{E_0\pi^3}\left(\frac{n}{n-1}\right)^{n/2}\frac{(n-1)^{1/2}}{n^2}(F^*-F)} + x^*. \tag{6b}$$

Substituting into Eq. (5) to obtain the values of the potential at the corresponding turning points, and taking the difference to calculate the barrier height gives:

$$\Delta E = \frac{4a}{3\pi\sqrt{nF^*}}(F^*-F)^{\frac{3}{2}} \tag{7}$$

so that:

$$\beta = \frac{3\pi}{4a}(nF^*)^{\frac{1}{2}}. \tag{8}$$

Thus, the combined potential shows identical asymptotic behavior for rigid sliding with a non-sinusoidal potential as with the classical PT model. The proportionality constant $\beta$ depends on the sharpness of the potential ($n$); a sharper potential has a higher value of $\beta$. This can also be written in terms of the curvature at the potential maximum (transition state), where $\chi_{TS} = \frac{1}{n}$, so that: $\beta = \frac{3\pi}{4a}\sqrt{\frac{F^*}{\chi_{TS}}}$. The plots in Fig. 3 compare exact numerical solutions (black dashed line) with those predicted by Eq. (7) (red solid line) for different values of $n$.

As expected, the agreement is good as $\Delta E$ approaches zero but deviates from the exact solution as $\Delta E$ increases. Note that there is no significant difference in this comparison between $n = 8$ and $n = 16$, suggesting that the value of the parameter $n$ does not significantly influence the accuracy of this approach. We also observed that as $n$ increases, the height of the energy barrier decreases more slowly with increasing force.

## 2.2 Lateral Force and Sliding Velocity

### 2.2.1 Transition Rates

In a contact with a sliding velocity $v$, the force $F$ adjusts to lower the activation barrier such that the transition rate $R$ increases to enable the system to transit the barrier at this

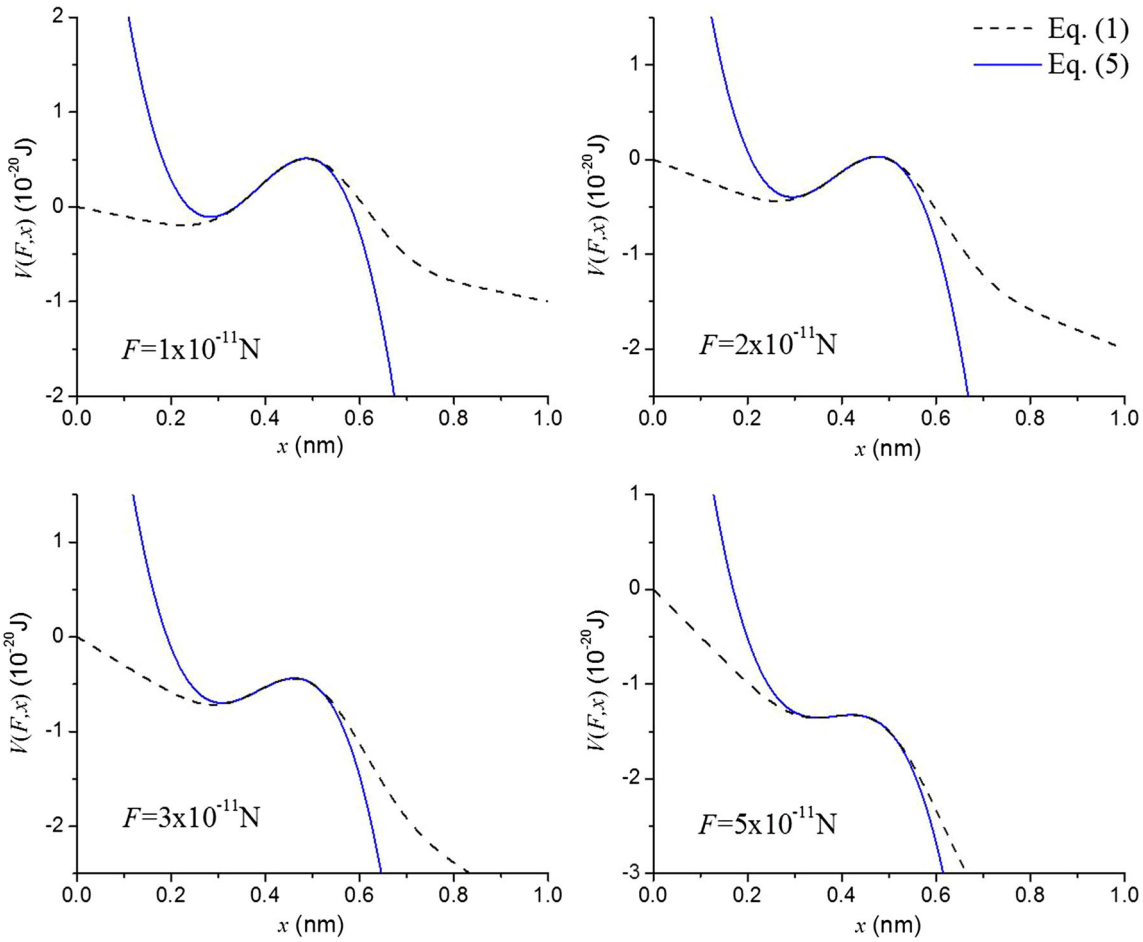


**Fig. 2** Comparison of Eq. (1) (*black dashed line*) and Eq. (5) (*blue solid line*) at different values of $F$ for a system with $n = 8$, $a = 1 \times 10^{-9}$ m and $E_0 = 1 \times 10^{-20}$ J. This indicates there is very good agreement between the two as the energy barrier approaches zero (Color figure online)

sliding velocity. If the periodicity along the sliding direction is $a$, then:

$$v = Ra \tag{9}$$

For a barrier height $\Delta E(F)$ under the influence of the external force $F$ that decreases as the force increases, then at some temperature $T$, the transition rate is given by:

$$R_{\mathrm{f}} = A \exp\left(-\frac{\Delta E(F)}{k_{\mathrm{B}}T}\right)\mu \tag{10}$$

where $R_{\mathrm{f}}$ represents the forward transition rate and $A$ is a pre-exponential factor (transition attempt frequency). The variable $\mu$ was introduced by Prandtl to capture the population density in the initial state [1]. For the shear of a contacting interface of a liquid, essentially all of the minima are occupied, so that $\mu \sim 1$. In the case of a nanoscale contact, where $a$ is the sliding distance from one minimum to the next and $\mu = 1$ (single contact), substituting into Eq. (9) gives:

$$v = aA \exp\left(-\frac{\Delta E(F)}{k_{\mathrm{B}}T}\right) \tag{11}$$

Note that if the activation energy in the absence of an external force, $E_0$, is small (a few times $k_{\mathrm{B}}T$), the system could diffuse back and forth between the adjacent minima in the absence of an external force, although the net motion would be zero. However, the possibility of backward transitions would be reflected in an increase in the lateral force to maintain the contact sliding at a certain velocity. In this case, Eq. (9) is modified to: $v = (R_{\mathrm{f}} - R_{\mathrm{b}})a$, where $R_{\mathrm{f}}$ and $R_{\mathrm{b}}$ are the forward and backward rates, respectively.

### 2.2.2 *Forward Transitions*

Assuming that only forward transitions take place gives:

$$\Delta E(F) = k_{\mathrm{B}}T \ln\left(\frac{v^*}{v}\right) \tag{12}$$

where $v^* = Aa$, and significant velocity dependences will only be seen for $v < v^*$. Explicit solutions depend on the form of $\Delta E(F)$. For $\Delta E = \frac{4a}{3\pi\sqrt{nF^*}}(F^* - F)^{\frac{3}{2}}$ this gives:

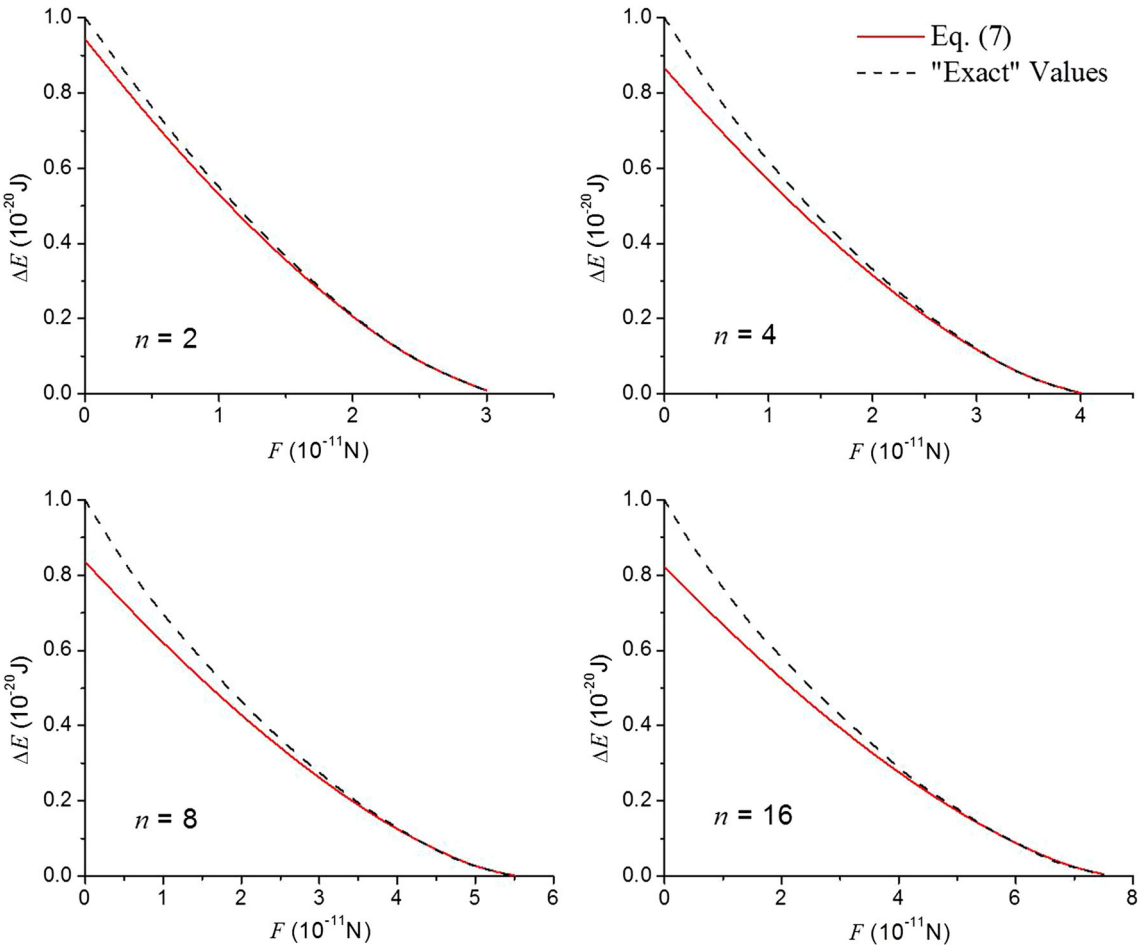


**Fig. 3** Variation of the energy barrier with force obtained from Eq. (7) (*red solid line*) and the exact solution (*black dashed line*), which shows that the agreement between the two curves improves as the energy barrier approaches zero (Color figure online)

$$F = F^* - \left(\frac{3\pi\sqrt{nF^*}k_BT}{4a}\right)^{2/3}\left(\ln\left(\frac{v^*}{v}\right)\right)^{2/3} \tag{13a}$$

and

$$\frac{1}{\beta k_BT}(F^* - F)^{3/2} = \ln\left(\frac{v^*}{v}\right). \tag{13b}$$

While Eq. (13b) is the same as the commonly reported PT model for a sinusoidal potential, in this expression, the sharpness of the non-sinusoidal potential ($n$) is captured by $\beta = \frac{3\pi}{4a}\sqrt{F^*n}$.

### 2.2.3 Forward and Backward Transitions

If backward transitions are taken into account, and assuming that the backward attempt frequency is also $A$, then $R_b = A\exp\left(-\frac{\Delta E_b(F)}{k_BT}\right)$, where $\Delta E_b$ corresponds to the energy barrier height for the backward transitions. Due to the shape of the overall potential $V(x, F)$ (Eq. 1), $\Delta E_b$ can be calculated as:

$$\Delta E_b = \Delta E_f + Fa. \tag{14}$$

An illustration of the energy barriers for forward and backward transitions is given in Fig. 4. With this picture, the rate becomes:

$$R_b = A\exp\left(-\frac{\Delta E_f(F) + Fa}{k_BT}\right) \tag{15}$$

and

$$\begin{aligned} v &= (R_f - R_b)a \\ &= aA\exp\left(-\frac{\Delta E_f(F)}{k_BT}\right)\left[1 - \exp\left(-\frac{Fa}{k_BT}\right)\right] \end{aligned} \tag{16a}$$

so that,

$$\frac{\Delta E_f(F)}{k_BT} = \ln\left(\frac{v^*}{v}\right) + \ln\left[1 - \exp\left(-\frac{Fa}{k_BT}\right)\right]. \tag{16b}$$

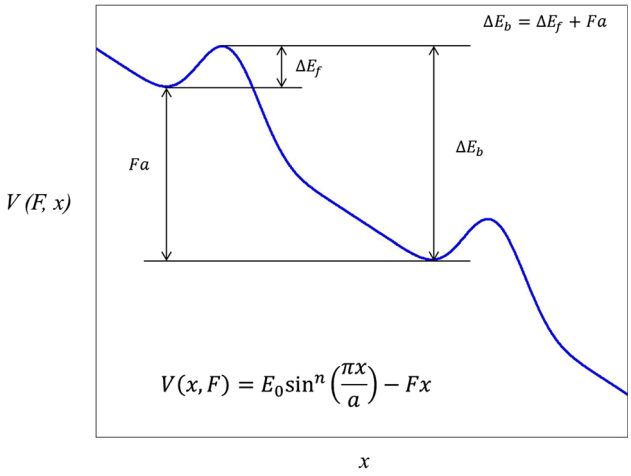


**Fig. 4** Illustration of the energy barriers for forward and backward transitions

Once again, for $\Delta E_f(F) = \frac{4a}{3\pi\sqrt{nF^*}}(F^* - F)^{\frac{3}{2}}$, this gives:

$$\frac{4a}{3\pi\sqrt{nF^*}k_BT}(F^* - F)^{\frac{3}{2}} = \ln\left(\frac{v^*}{v}\right) + \ln\left[1 - \exp\left(-\frac{Fa}{k_BT}\right)\right] \tag{17a}$$

$$\ln(v) = \ln(v^*) + \ln\left[1 - \exp\left(-\frac{Fa}{k_BT}\right)\right] - \frac{4a}{3\pi\sqrt{nF^*}k_BT}(F^* - F)^{\frac{3}{2}} \tag{17b}$$

This expression describes the velocity- and temperature-dependent lateral force associated with a non-sinusoidal potential of sharpness $n$.

### 2.3 Validation and Experimental Fit Example

In the previous sections, expressions for the lateral force applicable to any non-sinusoidal potential of the form $\sin^n(x)$ were derived, where $n$ is a measure of the sharpness of the potential. The use of these expressions is now demonstrated for a sliding contact with $n = 4$, $a = 1$ nm, $E_0 = 1 \times 10^{-20}$ J, and $A = 10{,}000$ Hz. The parameter $n = 4$ is chosen to describe a surface energy profile with moderate sharpness (see Fig. 1). The lattice constant ($a$) and energy barrier height ($E_0$) are of the order of typical metals and similar to values used in typical PT models [33, 34]. The transition attempt frequency ($A$) is chosen to be consistent with the order of magnitude of this parameter obtained by fitting the PT model to experimental friction versus sliding speed data [30]. The predicted relationship between velocity and lateral force for this system at different temperatures, assuming only forward (Eq. 13b) or forward and backward (Eq. 17b) transitions, is shown in Fig. 5. In order to corroborate the validity of these equations, Fig. 5 also shows the exact numerical solutions.

It can be observed that at low temperatures, neglecting the reverse transitions has only a small influence on the calculated sliding force, while, at higher sliding temperatures, this effect becomes quite large at low lateral forces. Note that, in all cases, there is excellent agreement with the exact solution when both forward and backward transitions are taken into account.

We can now analyze the effect of the sharpness of the potential on friction. Figure 6 shows the prediction of the model with both forward and backward transitions at $T = 298$ K for the same conditions as in Fig. 5 with different values of $n$. At low velocities, the three solutions are nearly identical. However, as the velocity increases, the model predictions diverge and indicate that friction will increase more slowly with velocity with sharper potential surfaces (larger $n$). This is consistent with the slower decrease in the height of the energy barrier with force shown in Fig. 3. This complements a recent study that showed the shape of the potential surface can affect transitions between thermal and a thermal friction regimes [35].

Now that the derivation of the proposed equations has been validated, Eq. (17b) is used to fit experimentally measured lateral force versus sliding velocity data obtained by AFM on a NaCl (001) surface under ultra-high vacuum conditions [36], to evaluate how close to sinusoidal the sliding potential is for this system. The authors were able to qualitatively describe the observed behavior by referring to the PT model but did not perform any fits to the experimental results. It should be noted that AFM experiments are usually not thought of as constant-force sliding scenarios. However, if the ratio between the tip–sample interaction and the elastic energy stored in the cantilever, which under the PT model is defined as $\gamma = 2\pi^2 E_0/k_L a^2$, is much greater than 1 (for example when using cantilevers with very low force constants), it is reasonable to assume that the variations in lateral force due to the deformation of the cantilever are small. Therefore, this can be approximated by constant-force sliding. In addition, if this is the case, the approximation should improve at relatively low sliding velocities, that is, away from the point at which friction becomes independent of sliding velocity, which seems to be the case of the results reported by Gnecco et al. [32].

Shown in Fig. 7 is the comparison between the experimental data for the velocity dependence ($\ln(v)$) of the lateral force ($F_L$) on a NaCl surface at normal loads of 0.44 (+) and 0.65 nN (×) [36], and the fits using Eq. (17b) (blue lines). The fits were performed at $T = 298$ $K$, fixing the value of $a$ at 0.47 nm, and having $E_0$ as a free parameter to account for possible changes in this value as a function of normal load in each case, while the values of $f_0$ and $n$ were tuned to obtained the best fit to both data sets as

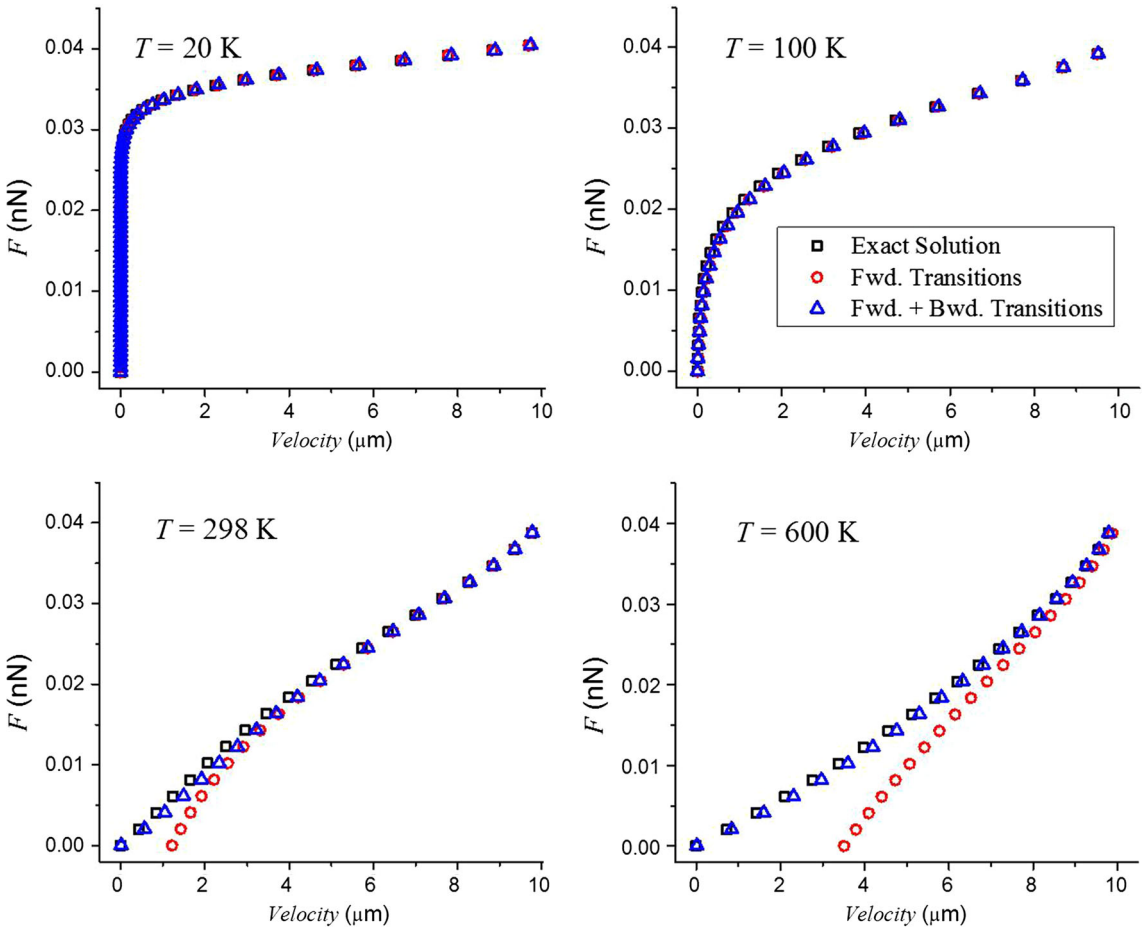


**Fig. 5** Relationship between sliding speed and lateral force at different temperatures predicted by the model assuming only forward (*red circles*) and both forward and backward (*blue triangles*) transitions, and the exact solution (*black squares*) for a non-sinusoidal potential with $n = 4$ (Color figure online)

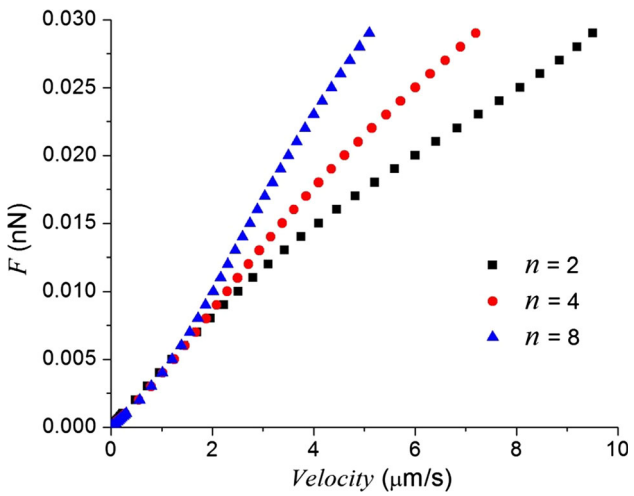


**Fig. 6** Effect of the potential sharpness $n$ on the rate of increase in friction with velocity predicted by the model with forward and backward transitions

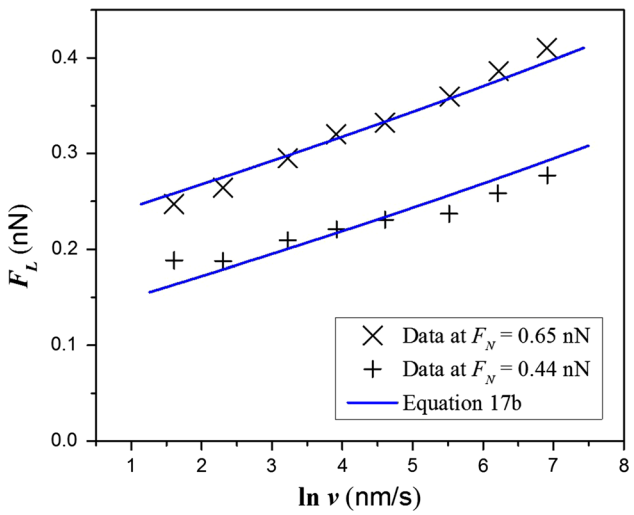


**Fig. 7** Comparison between the AFM experimental data obtained by Gnecco et al. [36] on a NaCl surface at a normal load of 0.65 (×) and 0.44 nN (+), and the fits obtained with Eq. (17b) (*blue lines*) (Color figure online)

a whole. This fitting procedure leads to values of $E_0$ of 0.59 and 0.70 eV for normal loads of 0.44 and 0.65 nN, respectively, and a value of $1 \times 10^7$ Hz for $f_0$ and $n = 2$. Note that these quantities are well within the normal experimental ranges found in AFM experiments. In addition, since the surface consists of a NaCl (001) crystal, it is expected to be well simulated by a not very sharp surface potential, so that $n = 2$ is also a reasonable fitting result.

## 3 Conclusion

An analytical solution is obtained for atomic-scale, constant-force sliding for a non-sinusoidal potential to gauge the influence of the shape of the potential on the variation in energy barrier with force; the validity of this solution is corroborated by the exact numerical solution. It is shown that the asymptotic behavior as the force approaches a critical value $F^*$ varies as $\Delta E(F) = \frac{1}{\beta}(F^* - F)^{3/2}$ as originally proposed by Prandtl. The value of the proportionality constant is found to vary as $1/\sqrt{\chi_{TS}}$, where $\chi_{TS}$ is the curvature at the potential maximum and $F^* = \frac{n\pi E_0}{a}\left(\frac{n-1}{n}\right)^{n/2}\left(\frac{1}{n-1}\right)^{1/2}$. The formula for $\Delta E(F)$ is used to calculate the velocity dependence of the friction force. The sharpness of the potential is found to affect the rate of increase in friction with velocity, particularly at fast velocities. The equation derived from the proposed model is then used to successfully fit one example of AFM experimental friction data. This analysis sets the stage for similar treatments with compliant sliding used in the atomic force microscope.

**Acknowledgments** We thank the National Science Foundation for support of this work under Grant No. CMMI-1265742.

## References

1. Prandtl, L.: Ein Gedankenmodell zur kinetischen Theorie der festen Körper. Z. Angew. Math. Mech. **8**, 85 (1928)
2. Tomlinson, G.A.: A molecular theory of friction. Phil. Mag. **7**, 905–939 (1929)
3. Erlandsson, R., Hadziioannou, G., Mate, C.M., McClelland, G.M., Chiang, S.: Atomic scale friction between the muscovite mica cleavage plane and a tungsten tip. J. Chem. Phys. **89**(8), 5190–5193 (1988)
4. Meyer, E.: Atomic force microscopy. Prog. Surf. Sci. **41**(1), 3–49 (1992)
5. Gnecco, E., Bennewitz, R., Gyalog, T., Loppacher, C., Bammerlin, M., Meyer, E., Güntherodt, H.J.: Velocity dependence of atomic friction. Phys. Rev. Lett. **84**(6), 1172–1175 (2000)
6. Gnecco, E., Bennewitz, R., Gyalog, T., Meyer, E.: Friction experiments on the nanometre scale. J. Phys.: Condens. Matter **13**(31), R619–R642 (2001)
7. Bennewitz, R., Gnecco, E., Gyalog, T., Meyer, E.: Atomic friction studies on well-defined surfaces. Tribol. Lett. **10**(1), 51–56 (2001)
8. Riedo, E., Gnecco, E., Bennewitz, R., Meyer, E., Brune, H.: Interaction potential and hopping dynamics governing sliding friction. Phys. Rev. Lett. **91**, 084502 (2003)
9. Socoliuc, A., Bennewitz, R., Gnecco, E., Meyer, E.: Transition from stick-slip to continuous sliding in atomic friction: entering a new regime of ultralow friction. Phys. Rev. Lett. **92**, 134301 (2004)
10. Furlong, O.J., Manzi, S.J., Pereyra, V.D., Bustos, V., Tysoe, W.T.: Kinetic Monte Carlo theory of sliding friction. Phys. Rev. B **80**, 153408 (2009)
11. Perez, D., Dong, Y.L., Martini, A., Voter, A.F.: Rate theory description of atomic stick-slip friction. Phys. Rev. B **81**, 245415 (2010)
12. Eyring, H.: Viscosity, plasticity, and diffusion as examples of absolute reaction rates. J. Chem. Phys. **4**(4), 283–291 (1936)
13. Kauzmann, W., Eyring, H.: The viscous flow of large molecules. J. Am. Chem. Soc. **62**(11), 3113–3125 (1940)
14. Eyring, H.: The activated complex in chemical reactions. J. Chem. Phys. **3**(2), 107–115 (1935)
15. Bell, G.: Models for the specific adhesion of cells to cells. Science **200**(4342), 618–627 (1978)
16. Konda, S.S.M., Brantley, J.N., Bielawski, C.W., Makarov, D.E.: Chemical reactions modulated by mechanical stress: extended Bell theory. J. Chem. Phys. **135**(16), 164103–164108 (2011)
17. Schallamach, A.: The velocity and temperature dependence of rubber friction. Proc. Phys. Soc. London, Sect. B **66**(5), 386–392 (1953)
18. Schallamach, A.: A theory of dynamic rubber friction. Wear **6**(5), 375–382 (1963)
19. Drummond, C., Israelachvili, J., Richetti, P.: Friction between two weakly adhering boundary lubricated surfaces in water. Phys. Rev. E **67**, 066110 (2003)
20. Mazuyer, D., Cayer-Barrioz, J., Tonck, A., Jarnias, F.: Friction dynamics of confined weakly adhering boundary layers. Langmuir **24**(8), 3857–3866 (2008)
21. Briscoe, B.J., Evans, D.C.B.: The Shear properties of Langmuir–Blodgett layers. Proc. R. Soc. Lond. A Math. Phys. Sci. **380**(1779), 389–407 (1982)
22. Tobolsky, A., Eyring, H.: Mechanical properties of polymeric materials. J. Chem. Phys. **11**(3), 125–134 (1943)
23. Dickinson, J.T., Park, N.S., Kim, M.W., Langford, S.C.: A scanning force microscope study of a tribochemical system: stress-enhanced dissolution. Tribol. Lett. **3**(1), 69–80 (1997)
24. Jacobs, T.D.B., Carpick, R.W.: Nanoscale wear as a stress-assisted chemical reaction. Nat. Nanotechnol. **8**(2), 108–112 (2013)
25. Gotsmann, B., Lantz, M.A.: Atomistic wear in a single asperity sliding contact. Phys. Rev. Lett. **101**, 125501 (2008)
26. Jacobs, T.B., Gotsmann, B., Lantz, M., Carpick, R.: On the application of transition state theory to atomic-scale wear. Tribol. Lett. **39**(3), 257–271 (2010)
27. Kopta, S., Salmeron, M.: The atomic scale origin of wear on mica and its contribution to friction. J. Chem. Phys. **113**(18), 8249–8252 (2000)
28. Liu, X.-Z., Ye, Z., Dong, Y., Egberts, P., Carpick, R.W., Martini, A.: Dynamics of atomic stick-slip friction examined with atomic force microscopy and atomistic simulations at overlapping speeds. Phys. Rev. Lett. **114**, 146102 (2015)
29. Spikes, H., Tysoe, W.: On the commonality between theoretical models for fluid and solid friction, wear and tribochemistry. Tribol. Lett. **59**(1), 1–14 (2015)
30. Li, Q., Dong, Y., Perez, D., Martini, A., Carpick, R.W.: Speed dependence of atomic stick-slip friction in optimally matched

experiments and molecular dynamics simulations. Phys. Rev. Lett. **106**, 126101 (2011)
31. Furlong, O.J., Manzi, S.J., Pereyra, V.D., Bustos, V., Tysoe, W.T.: Monte Carlo simulations for Tomlinson sliding models for non-sinusoidal periodic potentials. Tribol. Lett. **39**(2), 177–180 (2010)
32. Dong, Y., Perez, D., Gao, H., Martini, A.: Thermal activation in atomic friction: revisiting the theoretical analysis. J. Phys.: Condens. Matter **24**, 265001 (2012)
33. Manzi, S., Tysoe, W., Furlong, O.: Temperature dependences in the Tomlinson/Prandtl model for atomic sliding friction. Tribol. Lett. **55**(3), 363–369 (2014)
34. Dong, Y., Vadakkepatt, A., Martini, A.: Analytical models for atomic friction. Tribol. Lett. **44**(3), 367–386 (2011)
35. Djiha Tchaptchet, E., Djuidje Kenmoe, G.: Velocity and forced excitation effects on atomic friction force with deformable substrate. Nonlinear Dyn. 1–9 (2015). doi:10.1007/s11071-015-2210-2
36. Gnecco, E., Bennewitz, R., Socoliuc, A., Meyer, E.: Friction and wear on the atomic scale. Wear **254**(9), 859–862 (2003)